*Journal of The Electrochemical Society*, **150** (8) B367-B373 (2003)
0013-4651/2003/150(8)/B367/7/$7.00 © The Electrochemical Society, Inc.


# Raman Spectroscopy of Monolayers Formed from Chromate Corrosion Inhibitor on Copper Surfaces

**Belinda L. Hurley and Richard L. McCreery*,z**

*Department of Chemistry, The Ohio State University, Columbus, Ohio 43210-1185, USA*

Surface enhanced Raman scattering (SERS) was used to observe interactions of dilute $Cr^{VI}$ solutions with silver and copper surfaces *in situ*. Using silver as a model surface which supports strong SERS with a 514.5 nm laser, it was possible to observe $Cr^{III}$ at the near monolayer level, and the spectra were compared to those from $Cr^{III}$ oxyhydroxide species and $Cr^{III}/Cr^{VI}$ mixed oxide. Similar experiments were conducted with Cu surfaces and 785 nm excitation. Upon exposure to $Cr^{VI}$ solution, the characteristic Cu oxide Raman bands disappeared, and a $Cr^{III}$ band increased in intensity over a period of ~20 h. The intensity of the $Cr^{III}$ band on Cu became self-limiting after the formation of several $Cr^{III}$ monolayers, as supported by chronoamperometry experiments. This $Cr^{III}$ spectrum was stable after $Cr^{VI}$ was removed from the solution provided the potential remained negative of −200 mV *vs.* Ag/AgCl. The results support the conclusion that $Cr^{VI}$ is reductively adsorbed to Cu at the near neutral pH and open circuit potentials expected for Cu/Al alloys in field applications. The $Cr^{III}$ film is stable and is a strong inhibitor of electron transfer in general and oxygen reduction in particular. An important mechanistic feature of $Cr^{III}$ formation is the substitution lability of $Cr^{VI}$ compared to $Cr^{III}$. The $Cr^{VI}$-O bond can be broken much more rapidly than the substitution inert $Cr^{III}$-O bond, making formation of $Cr^{III}/Cr^{VI}$ mixed oxide kinetically favorable. Once reduced to $Cr^{III}$, however, the substitution inert oxyhydroxide film is much less labile. An important and central feature of $Cr^{VI}$ as a corrosion inhibitor is its transformation via reductive adsorption from a mobile, substitution labile $Cr^{VI}$ form to an insoluble, substitution inert $Cr^{III}$ oxyhydroxide. Furthermore, $Cr^{VI}$ reduction is likely to occur at cathodic sites previously responsible for oxygen reduction, which are then permanently blocked by a stable $Cr^{III}$ film with a thickness of a few monolayers.
 [DOI: 10.1149/1.1586923] 

Manuscript submitted October 2, 2002; revised manuscript received February 10, 2003. Available electronically June 16, 2003.

Currently, chromate conversion coatings (CCCs), and chromate-based barrier coatings and paints are preferred for the treatment of aluminum alloys because they provide both excellent adhesion properties and corrosion inhibition. Routine maintenance activities on these alloys, however, are a large source of environmentally hazardous waste containing the hexavalent chromium present in these coatings. Hexavalent chromium is a danger to worker health and its use has been limited or prohibited by various local, state, and federal regulations. In the search for suitable nonchromate replacements, a basic understanding of the mechanism by which chromate-based protection systems provide such excellent protection will be invaluable.

Considerable research has centered on the use of chromate conversion coatings on aluminum aircraft alloy AA-2024 T3 which contains, by weight, 3.8-4.9% copper, 1.2-1.8% magnesium, and less than 1% each of other trace metals, the balance being aluminum.[1] All of the AA-2XXX series alloys are prone to corrosion, particularly pitting and stress corrosion cracking, arising from the inhomogeneous distribution of copper in these alloys.[2] This distribution leads to the establishment of local galvanic cells between copper-rich and copper-poor areas and thus destructive localized corrosion. Approximately 60% of the secondary phase intermetallic particles found in AA-2024 T3 are copper-rich $Al_2CuMg$.[2] CCCs such as commercially available Alodine 1200 form a corrosion-inhibiting film on both the matrix and the intermetallics of AA-2024 T3.[3,4] The mechanism by which a CCC film protects AA-2024 T3, however, is not fully understood. In an attempt to better understand the relationship between CCCs and copper-rich intermetallics, previous studies in this laboratory were undertaken with pure copper exposed to $Cr^{VI}$ in solution.[5,6] These studies indicate that $Cr^{VI}$ inhibits the cathodic activity of copper in aluminum alloys, particularly toward oxygen reduction.

The current approach uses Raman spectroscopy, specifically surface enhanced Raman scattering (SERS), to investigate the formation of $Cr^{III}$ oxyhydroxide on pure copper. Unlike many surface techniques, Raman spectroscopy probes molecular structure in addition to speciation. Additionally, it is nondestructive and *in situ* analysis is straightforward, providing a means to acquire spectra under potential control. Spectral enhancement factors of greater than $10^6$ are obtainable with SERS on silver, gold, and copper.[7] Because of the SERS enhancement, the molecular structure of even a monolayer of a Raman active species on roughened copper can be probed.[8] In fact, it is the scattering of molecules on the first layer of a surface that receives the greatest enhancement.[7] The effect diminishes significantly with increasing distance from the surface. Therefore, not only is the immediate surface spectrum enhanced, but interference from species not on the immediate surface is minimized. Silver was initially used as a model in this study to better understand the formation of a $Cr^{III}$ oxyhydroxide and/or a $Cr^{III}/Cr^{VI}$ mixed oxide from $Cr^{VI}$ in solution. Subsequent experiments were then performed on copper. Previous work in this laboratory provided coulombic evidence of the formation of a near-monolayer $Cr^{III}$ film on copper exposed to solution $Cr^{VI}$.[6] This work provides an *in situ* spectroscopic probe of the formation and structure of this film.

## Experimental

*Materials.*—All chemicals were reagent grade and were used as received. Potassium sulfate, potassium hydroxide, and sodium hydroxide were obtained from Mallinckrodt; potassium dichromate and chromium(III) nitrate from Alfa Aesar; cupric sulfate, anhydrous powder from J. T. Baker; silver nitrate from Fisher Scientific; and chromium potassium sulfate (chrome alum) from Allied Chemical. All solutions were prepared and rinsing was performed with Barnstead Nanopure water, 17.8 MΩ minimum resistivity. The silver substrate was 99.9985% silver foil, 0.1 mm thick, obtained from Johnson Matthey Materials Technology. Unless otherwise noted, the copper substrate was 99.99% copper sheet, 1.0 mm thick, obtained from Alfa Aesar. A 99.999%, 5.0 mm diam copper rod was obtained from Goodfellow. AA-2024 T3 sheet, 0.025 in (0.064 mm) thick, was obtained from ALCOA.

Various chromium compounds were prepared using the methods described by Xia *et al.*[9] $Ag_2CrO_4$ was prepared by dissolving 0.4 g $K_2Cr_2O_7$ in 50 mL $H_2O$ and then adding 1.3 g $AgNO_3$. The precipitate, $Ag_2CrO_4$, formed immediately and was filtered, rinsed with $H_2O$, and air dried. $Cr(OH)_3$ was prepared by dissolving 4.0 g $Cr(NO_3)_3 \cdot 9H_2O$ in 25 mL $H_2O$; 1 M KOH was added dropwise to the stirred solution until the pH reached 4.5. The precipitate,

* Electrochemical Society Active Member.
z E-mail: mccreery.2@osu.edu

$Cr(OH)_3$, was filtered, rinsed with $H_2O$, and air dried. The $Cr^{III}/Cr^{VI}$ mixed oxide was prepared by dissolving 4.0 g $Cr(NO_3)_3 \cdot 9H_2O$ and 0.5 g $K_2Cr_2O_7$ in 50 mL $H_2O$; 1.0 M NaOH was added dropwise to the stirred solution until the pH exceeded 4.5. The mixed oxide precipitate was filtered, rinsed with $H_2O$, and air dried. Concentrated $Cr^{VI}$ solutions added to electrochemical cells were prepared with $K_2Cr_2O_7$ and $H_2O$.

*Instrumentation*.—In all cases the reference electrode was Ag/AgCl (Bioanalytical Systems) and the auxiliary electrode was a platinum wire. All noted potential values are *vs.* Ag/AgCl. Oxidation/reduction cycles (ORCs) for roughening of the silver foil electrode and the copper rod were performed with a Bioanalytical Systems 100B electrochemical workstation. Copper sheet deposition roughening and chronoamperometry were performed with a Gamry PC3/300 potentiostat. All *in situ* potentiostatic control was performed with a Bioanalytical Systems model PWR-3 potentiostat.

Raman spectra on the silver substrate were acquired with a 514.5 nm laser on an f/1.5 Kaiser spectrograph with a holographic grating, 180° backscattered geometry with a laser spot size of ~50 μm. A video charge coupled device (CCD) camera was used to focus the laser at low power (<200 μW) on the silver foil. Spectra were acquired with 5 mW of laser power at the sample and were not intensity corrected for instrumental response. Raman spectra of the copper sheet substrate were acquired with a 785 nm laser with a Chromex Raman 2000 spectrograph equipped with a 600 line/mm grating optimized at 1000 nm and an Olympus 40 times magnification/0.80 W immersible objective giving a spot size of ~3-4 μm with 10 mW of laser power provided at the sample. A Logitech QuickCam was used for focusing. Raman spectra of the copper rod substrate were acquired with macro optics consisting of a gold coated, off-axis paraboloidal reflector installed in the same Chromex Raman 2000 spectrograph with 785 nm excitation. The laser spot size was ~50 μm with 50 mW of laser power provided at the sample. Focal position was determined by maximizing the intensity of the $Cu_2O$ bands discussed below. All spectra acquired with the Chromex Raman 2000 were intensity corrected using National Institute of Standards and Technology standard SRM2241 and the method described by Ray *et al.*[10,11] Both the Kaiser and the Chromex spectrographs were equipped with liquid nitrogen cooled CCD detectors cooled to −110 and −90°C, respectively. Integration times for all spectra were 30 s or less.

X-ray photoelectric spectroscopy was performed with a VG Scientific Escalab MKII system with a Mg Kα source across a range of 0 to 1000 eV binding energy. An Orion model 520 A pH meter was used to determine pH values. Absorbance spectra of aliquots of $Cr^{VI}$ solutions from the various electrochemical cells were acquired with a Perkin-Elmer Lambda 900 UV/Vis spectrometer. Concentrations were determined using the Xia *et al.* previously determined molar absorptivity of $\epsilon_{339nm} = 1.49 \times 10^3\ M^{-1}\ cm^{-1}$.[12]

*Sample preparation and spectral acquisition*.—*Reference spectra*.—Raman spectra of solid $Ag_2CrO_4$, solid $Cr(OH)_3$, and solid synthetic $Cr^{III}/Cr^{VI}$ mixed oxide were acquired with 514.5 nm light on the Kaiser spectrometer noted above. Solid $Cr_2O_3$ was mixed with 100 mM $K_2SO_4$ to make a paste before spectral acquisition with the same spectrometer. A Raman spectrum of solid chrome alum (not shown) was acquired with the Chromex spectrometer noted above.

*Silver substrate*.—SERS requires that the surface of the substrate be roughened in order to promote enhancement. To this end, the silver foil was cut to a strip approximately 0.9 × 9.0 cm, abraded with successive grits of silicon carbide papers (Buelher P2400, P4000) wetted with Nanopure water and rinsed. The ORC used to roughen the foil was adapted from the procedure of Weaver *et al.* and consisted of a scan from −400 to +600 mV, a hold at +600 mV for 1 s, a scan from +600 to −400 mV and then a hold at −400 mV for 10 s.[8] The scan rate was 100 mV/s. This cycle was repeated 20 times in 5 mL of 100 mM potassium sulfate. Approximately 1 $cm^2$ of the silver foil was submerged in the electrolyte during roughening. Upon completion of the ORC roughening, the cell was disconnected from the workstation, but the electrodes were left in the ORC solution. The cell was properly positioned in the Raman spectrometer and connected to the potentiostat. The electrochemical cell employed was a 1 × 5 × 5 cm quartz cuvette and all spectra were acquired through a 5 × 5 cm face.

*Copper substrate*.—The copper sheet was cut into a 1 $cm^2$ piece and a copper wire was attached to one side with silver epoxy resin (SPI Supplies/Structure Probe, Inc.). The assembly was then embedded in epoxy (Buelher) leaving the smooth side exposed. This copper electrode was hand-polished with successive grits of silicon carbide papers wetted with Nanopure water (Buelher 240, 400, 600, P2400, P4000) and then rinsed in $H_2O$. Electrochemical copper deposition was used to roughen of the surface, which promotes the SERS effect. Using a method adapted from Kudelski *et al.*, deposition was accomplished by suspending the electrode face down in an unstirred solution of 500 mM cupric sulfate and holding it at a potential of −100 mV for 45 min.[13] Immediately after deposition all three electrodes were rinsed and placed in a crystallizing dish (80 mm diam, 40 mm height) which served as the electrochemical cell. The electrolyte was 100 mM potassium sulfate. The copper electrode was arranged with its surface facing up and spectra were acquired through the solution covering the electrode with an immersible objective.

In experiments employing a copper rod as the electrode, the end of the rod was cut at a 45° angle and the rod was enclosed in Teflon shrink tubing (Small Parts Inc.) leaving the beveled face exposed. This beveled face was hand-polished with successive grits of silicon carbide papers (Buelher 240, 400, 600, P2400, P4000) wetted with Nanopure water and then rinsed. Using a method adapted from Weaver *et al.*, roughening was performed with ORCs consisting of a scan from −1000 to +400 mV, a hold at +400 mV for 1 s, a scan from +400 to −1000 mV and then a hold at −1000 mV for 10 s.[8] The scan rate was 100 mV/s. This cycle was repeated 20 times in 10 mL of 100 mM potassium sulfate in a 1 × 5 × 5 cm quartz cell. The cell was disconnected from the workstation with the electrodes remaining in the ORC solution, positioned in the Raman spectrometer and connected to the potentiostat. Spectra were acquired through a 5 × 5 cm face with the rod's beveled face at a 45° angle to the cell face.

## Results and Discussion

*In situ SERS of silver exposed to chromate*.—As a result of the SERS effect, spectroscopic detection of a monolayer or even a submonolayer of a Raman active species on silver is not uncommon.[14] Silver was, therefore, used first as a model to obtain *in situ* Raman spectra of a metal exposed to $Cr^{VI}$ in solution. Figure 1 shows four overlaid, *in situ* spectra of the surface of the silver substrate in the electrochemical cell at $t = 0$ (in $K_2SO_4$ solution immediately before addition of $Cr^{VI}$) and at $t = 2$, 10, and 30 min after 100 mM $Cr^{VI}$ solution was added to the cell for a final concentration of 5.6 mM $Cr^{VI}$. Baselines on the spectra have not been adjusted or offset. During acquisition of these spectra no potential was applied, thus allowing the silver foil to remain at its open circuit potential (OCP) of approximately +175 mV *vs.* Ag/AgCl in 100 mM $K_2SO_4$. The first obvious changes in the spectrum acquired 2 min after the addition of $Cr^{VI}$ are a small feature in the region between 530 and 670 $cm^{-1}$ and a more prominent band between 730 and 890 $cm^{-1}$. With time, both bands in these regions grow. After about 10 min, the higher energy band began to decrease in size and the lower energy band continued to grow. Within 15 min (not shown) the lower energy band clearly dominated the spectrum. The spectrum showed little change between 15 and 30 min.

The specific identities of the species giving rise to these two bands are not easily assigned, but previous work with metal surfaces (including silver) exposed to chromate, along with the experimental

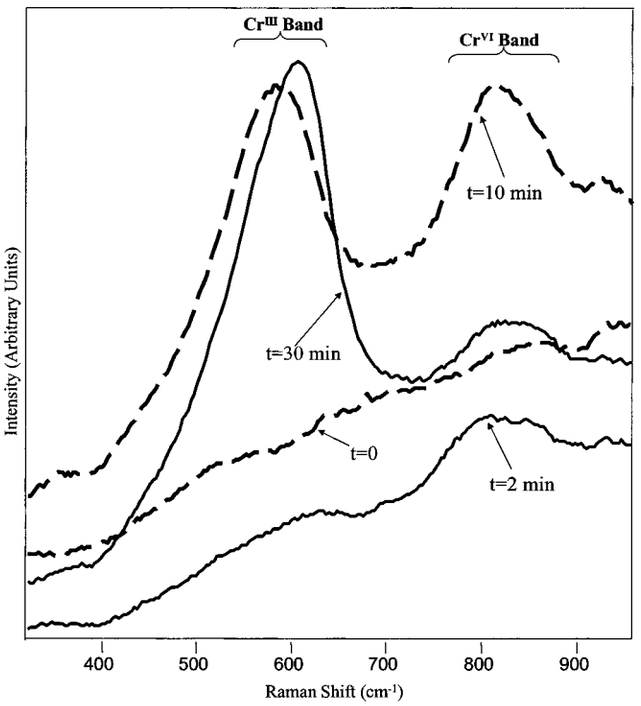


**Figure 1.** *In situ* SER spectra of silver substrate at open circuit potential, before ($t$ = 0, in 100 mM $K_2SO_4$) and after exposure to $Cr^{VI}$ (in 100 mM $K_2SO_4$, 5.6 mM $Cr^{VI}$). See text for details.

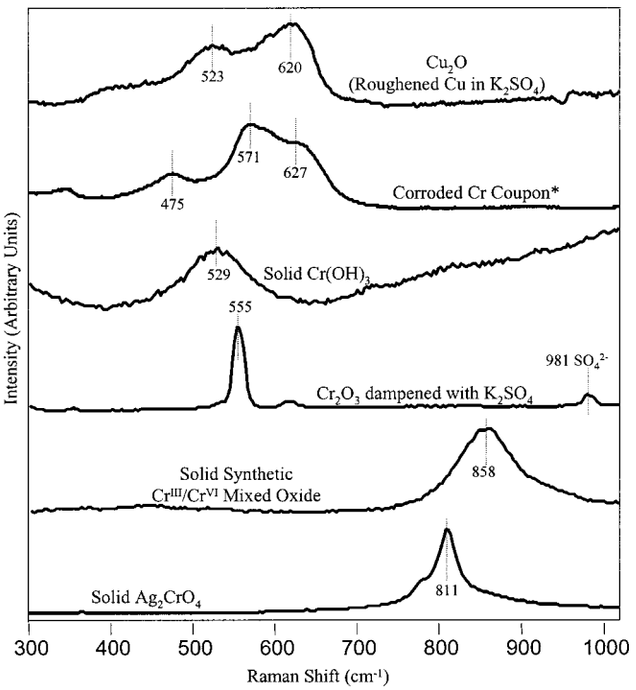


**Figure 2.** Reference Raman spectra. $Cu_2O$, 785 nm excitation (Chromex spectrometer); Corroded Cr Coupon with broad band between 535 and 665 $cm^{-1}$ attributed to a $Cr^{III}$ species with significant contributions from α-CrOOH, 647.1 nm excitation; solid $Cr(OH)_3$, $Cr_2O_3$ dampened with $K_2SO_4$, solid synthetic $Cr^{III}/Cr^{VI}$ mixed oxide, and solid $Ag_2CrO_4$, 514.5 nm excitation (Kaiser spectrometer). *Adapted from Reference 19, with permission.

conditions, leads to the assumption that they are some type of chromium surface species.[4,6,9,15] X-ray photoelectron spectroscopy (XPS) analysis of the surface of silver foil subjected to identical treatment showed carbon, oxygen, silver, sulfur, and chromium at atomic percentages of 1.00:0.37:0.22:0.03:0.02, respectively. Speciation of chromium with XPS analysis, however, is unreliable as photoreduction of $Cr^{VI}$ to $Cr^{III}$ has been observed.[16,17] Furthermore, two details indicate that these bands originated from surface and not solution species. Both dichromate and bichromate were present in 5.6 mM $Cr^{VI}$ at the cell pH of ~5 and these species produce a strong sharp band at ~900 $cm^{-1}$.[18] Slight defocussing of the laser spot while acquiring the spectra of Fig. 1 caused appearance of a sharp 900 $cm^{-1}$ peak on top of the broad surface scattering. The absence of the 900 $cm^{-1}$ peak with proper focus indicates that the majority of the scattering was collected from the surface rather than the solution. Additionally, when the silver electrode was removed from the cell, rinsed and allowed to dry in room air, the same two bands (slightly shifted, but still strong) were present in spectra acquired of the dry electrode. The shift in peak frequencies of these bands is likely due to changes in hydration of $Cr^{III}$, and accompanying changes in the relative abundance of water and hydroxide coordination. Assuming these two broad bands are attributable to chromium surface species, comparison to the reference spectra in Fig. 2 implies that the lower energy band arose from a $Cr^{III}$ species and the higher energy band arose from a $Cr^{VI}$ species. The reference spectrum from Maslar *et al.* of a corroded chromium coupon especially shows the broad nature of a $Cr^{III}$ oxyhydroxide band.[19] Maslar *et al.* acquired both Raman spectra and X-ray diffraction (XRD) patterns of the same corroded chromium coupon. The XRD patterns were identified through comparison to the JCPDS International Center for Diffraction Data. By combining the XRD data with the Raman data they attributed the broad band between 535 and 665 $cm^{-1}$ in Fig. 2 to a $Cr^{III}$ species with significant contributions from α-CrOOH. Oblonsky *et al.* also acquired SERS spectra of passive films formed on chromium samples.[20] These spectra contained a broad band centered at 600 $cm^{-1}$ which was tentatively attributed to $Cr(OH)_2$, CrOOH or a species with no bulk analog. Likewise, the Melendres *et al.* SERS spectra of chromium samples corroded in NaCl exhibit a broad band centered at ~580-590 $cm^{-1}$.[21] Furthermore, both the Maslar *et al.* work and previous work in this lab have attributed bands in the region from 750 to 950 $cm^{-1}$ to $Cr^{VI}$-O stretches, as can be seen in the spectrum of $Cr^{III}/Cr^{VI}$ mixed oxide in Fig. 2.[9,22] It should be noted that the cross section of $Cr^{VI}$-O scattering is generally much larger than that of $Cr^{III}$ oxyhydroxide vibrations and, therefore, the area of the bands is not a direct indicator for quantitative comparison.[19] Furthermore, the amorphous nature of $Cr^{III}$ films, the degree and type of hydration, and the specific placement and amount of $Cr^{VI}$ within these films all contribute to their broadening and slight variations in Raman shift.[9,19,20] The distribution of components and band profiles of both the 400-600 and the 700-900 $cm^{-1}$ bands are likely to depend on sample history, pH, and composition.

Finally, as further evidence that these two bands originate from $Cr^{III}$ and $Cr^{VI}$ species, the cell was flushed to obtain a $Cr^{VI}$ concentration of <60 μM. The spectrum of the electrode in the flushed cell was virtually identical to that at $t$ = 30 min in Fig. 1. Upon the application of a potential of −1000 mV, however, the higher energy band (attributed to $Cr^{VI}$) nearly disappeared and the lower energy band (attributed to $Cr^{III}$) broadened, increased slightly in area, and shifted downward about 20 $cm^{-1}$. An electrochemical experiment was conducted with silver foil in all ways identical to the above Raman experiment with the following exception. After roughening, rather than positioning the cell in the spectrometer, a chronoamperometry experiment was performed with the foil held at +177 mV (the approximate OCP of the silver foil prior to the $Cr^{VI}$ injection during the Raman experiment). Using the Clark *et al.* estimate that the three-electron reduction of $Cr^{VI}$ to form a $Cr^{III}$ monolayer re-

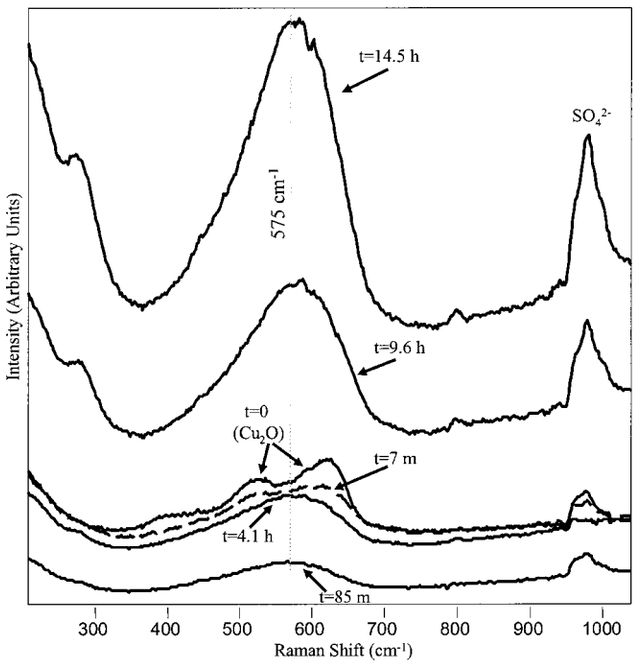


**Figure 3.** *In situ* SER spectra of copper substrate at −200 mV, before ($t$ = 0, in 100 mM $K_2SO_4$) and after exposure to $Cr^{VI}$ (in 100 mM $K_2SO_4$, 5.8 mM $Cr^{VI}$). See text for details.

quires $1.6 \times 10^{-3}$ C/$cm^2$, the integrated area of the reduction current produced upon injection of $Cr^{VI}$ solution indicated the formation of slightly more than a monolayer of $Cr^{III}$ 2 min after injection and slightly less than two monolayers 10 min after injection.[6]

*In situ SERS and chronoamperometry of copper exposed to chromate*.—As noted above, copper comprises approximately 4% of AA-2024 T3, with the copper-rich intermetallics providing undesirable cathodic sites to drive the oxidative dissolution of the aluminum matrix.[1,2] Previous work in this laboratory concluded that chromate inhibits cathodic reactions on copper surfaces, particularly oxygen reduction.[6] It was theorized that the reduction of $Cr^{VI}$ forms a film of $Cr^{III}$ on the surface which occupies oxygen adsorption sites and acts as a barrier to electron transfer. Figure 3 shows the overlaid, *in situ* Raman spectroscopic progression of the formation of a chromium containing film on a copper electrode held at a potential of −200 mV, the approximate measured OCP of AA-2024 T3 in 100 mM $K_2SO_4$. Again, the spectra were not baseline corrected and share the same intensity scale. At $t$ = 0 (in $K_2SO_4$ before addition of $Cr^{VI}$), the spectrum is identical to roughened copper at its OCP in 100 mM $K_2SO_4$ (Fig. 2, top spectrum). In a separate experiment, the same electrode, subjected to the same pretreatment, was held at −200 mV for more than 15 h in 100 mM $K_2SO_4$. The spectrum remained the same as the "$t$ = 0 spectrum" shown in Fig. 3 throughout those 15 h. It has been clearly established that the bands centered at ~523 and ~620 $cm^{-1}$ arise from surface $Cu_2O$.[8,23-26] These same bands are also present on spectra of dry, unroughened copper (not shown). Coincidentally, the broad, overlapping $Cu_2O$ bands bracket the range of most $Cr^{III}$ oxyhydroxide species. The series of spectra in Fig. 3 acquired over a period of 14.5 h after the $Cr^{VI}$ addition, however, shows a definite loss of $Cu_2O$ character and an increase in a band centered at 575 $cm^{-1}$. Immediately after acquisition of the $t$ = 0 spectrum, 800 mM $Cr^{VI}$ was added to give a cell concentration of 5.8 mM $Cr^{VI}$. 7 min after the addition, the resolution of the two $Cu_2O$ bands was severely diminished, and within 85 min, they cannot be discerned in the spectrum. Also, within 85 min, the 575 $cm^{-1}$ band clearly starts to appear. Spectra at 4.1, 9.6, and 14.5 h show this band's continued growth. The experimental conditions and comparison to the reference spectra, particularly the spectrum of the corroded chromium coupon, strongly imply that the band at 575 $cm^{-1}$ results from the scattering of a $Cr^{III}$ oxyhydroxide species with a significant contribution from α-CrOOH.[19]

As in the case of the silver SERS spectra, the copper SERS spectra do not show the solution chromate band at 900 $cm^{-1}$, indicating that the scattering is predominantly that of surface species. Additionally, a separate experiment was conducted in a manner identical to the experiment represented in Fig. 3, producing similar spectra. At the conclusion of the experiment, the electrode was removed from the cell, rinsed, and dried in room air. A spectrum of the dried electrode still showed the band attributed to $Cr^{III}$ although it had broadened slightly and was unsymmetric with a maximum intensity at 533 $cm^{-1}$ and a broad shoulder at ~575 $cm^{-1}$. The band centered at 533 $cm^{-1}$ suggests an increase in $Cr(OH)_3$ character as seen in the reference spectrum of $Cr(OH)_3$ (Fig. 2) which has a broad band centered at 529 $cm^{-1}$. An increase in $Cr(OH)_3$ character is supported by Sunseri *et al.*, who conducted photocurrent spectroscopic analysis of passive films on chromium and attributed the different compositions in these films to $Cr^{III}$ oxides in various states of hydration.[27] As in the Maslar *et al.* work, the Sunseri *et al.* analysis differs from the present work in that the $Cr^{III}$ oxyhydroxide was formed from the oxidation of chromium rather than the reduction of $Cr^{VI}$. In general, however, their work concluded that increasing pH or decreasing potential leads to a more hydrated $Cr^{III}$ species on the surface. If a species similar to CrOOH is indeed predominant on the electrode before rinsing, then removing the electrode from the slightly acidic cell (pH ~ 5) and rinsing with water would subject it to an increased pH and, therefore, lead to an increase of $Cr(OH)_3$ character.

One notable difference between the silver substrate spectra and the copper substrate spectra is the absence of any definite $Cr^{VI}$ band in the copper data. *In situ* SERS spectra were also acquired in two separate experiments with a roughened copper rod substrate in which the rod was first held at −1000 mV in 100 mM $K_2SO_4$ for several minutes, potential control was removed, and 800 mM $Cr^{VI}$ was added to the cell for a final concentration of ~40 mM $Cr^{VI}$. In both these experiments, immediately upon addition of $Cr^{VI}$, a band appeared at 855 $cm^{-1}$ and remained for a minimum of 10 min. Synthetic $Cr^{III}/Cr^{VI}$ mixed oxide (Fig. 2) has a broad band at 858 $cm^{-1}$. As discussed above, this band is attributed to the stretches of $Cr^{VI}$-O bridging bonds.[9,22] Assuming that the band seen at 855 $cm^{-1}$ is also due to the $Cr^{VI}$-O stretch, it is reasonable to assert that $Cr^{VI}$ species can form on copper and that they can be detected with Raman spectroscopy. Although no such band appeared in spectra of the copper substrate in the experiments described in the preceding paragraphs, a small band at 800 $cm^{-1}$ can be detected in Fig. 3 in the spectra acquired at $t$ = 9.6 h and $t$ = 14.5 h. The small band is not currently identified, but several $Cr^{VI}$ species scatter in that general region and it is possible that the small 800 $cm^{-1}$ band arose from some type of $Cr^{VI}$ species.[9,22]

Two other bands in Fig. 3 merit discussion. The band appearing late in the series at 273 $cm^{-1}$ is possibly due to $Cl^-$ contamination from the reference electrode. Several metal-chloride stretches appear in this region including Cr-Cl at 268 and Cu-Cl at 290 $cm^{-1}$.[8,28] When the cell was manually flushed with 100 mM $K_2SO_4$ while maintaining potential control, the band at 273 $cm^{-1}$ disappeared. The band at 978 $cm^{-1}$ is attributed to the presence of sulfate within the film. Spectra of the sulfate electrolyte show its totally symmetric stretch as a strong, sharp band at 981 $cm^{-1}$ while the spectrum of chromium alum exhibits this stretch at 987 $cm^{-1}$. Pejov *et al.* assigned a band centered at 974.8 $cm^{-1}$ to sulfate ions doped in $K_2CrO_4$.[29] It seems probable that the broad nature of the sulfate band shown in Fig. 3 indicates the presence of several sulfate spe-

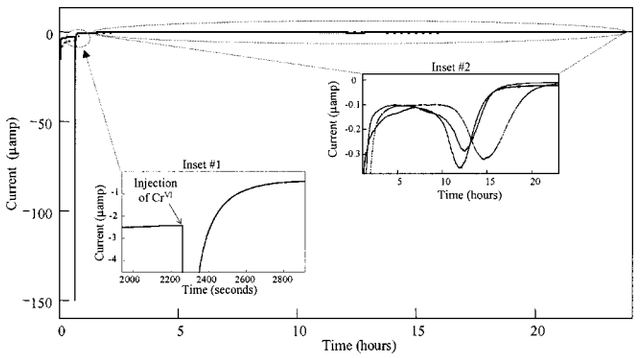


**Figure 4.** Chronoamperometry data of copper electrode in 100 mM $K_2SO_4$ at −200 mV before and after injection of $Cr^{VI}$. Final $[Cr^{VI}] \approx 5.5$ mM. Experiments (1) solid; (2) dotted; (3) gray. (Inset 1 shows experiment 1 only.)

cies. No sulfate band was present until the addition of $Cr^{VI}$ to the cell. Immediately after the addition of $Cr^{VI}$, however, it appeared and its intensity continued to track that of the $Cr^{III}$ band throughout the experiment. The proportion of the sulfate band to the $Cr^{III}$ band remained approximately the same after the cell was flushed, as was the case for spectra of the dry copper electrode acquired at the completion of the above experiments after rinsing and drying in room air. Although this evidence indicates that sulfate ions are situated within the film, they are not necessarily required for the growth of the $Cr^{III}$ oxyhydroxide film. A SERS experiment was performed in all ways identical to the experiment which produced the spectra in Fig. 3 with two exceptions; the electrolyte was 100 mM NaCl and the electrode was held at −540 mV, the approximate OCP of AA-2024 T3 in 100 mM NaCl. Spectra from this experiment showed the same slow growth of a virtually identical $Cr^{III}$ band, albeit slightly shifted to a center of 566 $cm^{-1}$ compared to a center of 575 $cm^{-1}$ for the $K_2SO_4$ experiments.

Figure 4 shows the results of chronoamperometry experiments with a copper electrode subjected to identical conditions as those used in the SERS experiment which produced the spectra of Fig. 3. This experiment was performed three times over a period of one month to test reproducibility. Additionally, each experiment was started at a different time of the day to exclude the possibility of environmental influence such as light and temperature fluctuations. The electrode was roughened and the cell was established as noted above with the copper electrode held at −200 mV. After 37.6 min, 800 mM $Cr^{VI}$ was injected to bring the cell concentration to ~5.5 mM $Cr^{VI}$. As in similar experiments performed by Clark *et al.*, after the injection a large reduction spike appeared, indicating the reduction of $Cr^{VI}$ to $Cr^{III}$ on the electrode surface.[6] Combining the chronoamperometry experiments with the SERS experiment supports the theory that the formation of a $Cr^{III}$ film inhibits the reduction of oxygen through adsorption to oxygen reduction sites. The reduction current before injection of $Cr^{VI}$ to the cell has been attributed to oxygen reduction.[6] 7 min after the $Cr^{VI}$ injection, at the same time that the SERS spectrum started to show a loss of $Cu_2O$ character, the reduction current had decreased by 74% in experiment 1, 60% in experiment 2, and 85% in experiment 3 compared to the current before the $Cr^{VI}$ injection. After 85 min, when the SERS spectrum showed no discrete $Cu_2O$ bands and the 575 $cm^{-1}$ band was established, the reduction current had decreased by 91, 93, and 97%, respectively. Table I outlines the reduction current for experiment 1. As can be seen in Fig. 4, outlines for experiments 2 and 3 would be very similar.

Inset 2 of Fig. 4 shows an unexpected but reproducible temporary increase in current beginning approximately 6-10 h after the injection of $Cr^{VI}$. Although observed in all three experiments, in the interest of brevity only experiment 1 is discussed. The integrated area between 6.3 and 16.9 h (from the time of injection) is slightly more than twice the integrated area of the initial reduction spike measured from the time of injection to 5.7 min after the injection. Again, the Clark *et al.* estimation of $1.6 \times 10^{-3}$ $C/cm^2$ or 5.4 $nmol/cm^2$ for the formation of a $Cr^{III}$ monolayer from $Cr^{VI}$ solution was used to estimate the coverage of the $Cr^{III}$ film.[6] Assuming that both the initial spike and the later temporary increase in reduction current are due to reduction of $Cr^{VI}$, approximately a monolayer of a $Cr^{III}$ film ($1.45 \times 10^{-3}$ $C/cm^2$ or 5.0 $nmol/cm^2$) was established in the first 5.7 min after the injection and the equivalent of approximately two more layers ($3.10 \times 10^{-3}$ $C/cm^2$ or 10.7 $nmol/cm^2$) was established during the later temporary increase in current. Integration of the late temporary increase in current in the other two experiments indicate similar results, with an additional 4.47 $10^{-3}$ C (15.4 $nmol/cm^2$) and $3.75 \times 10^{-3}$ C (13.0 $nmol/cm^2$) passed for experiments 2 and 3, respectively. All integrated areas were calculated using baselines tangent to the data. Presumably, $Cr^{VI}$ was also slowly reduced after establishment of the approximate monolayer and before the current increase. Uncertainty as to the amount of current due to oxygen reduction, however, precludes the quantitative calculation of the amount of $Cr^{VI}$ reduced during this period. There is additional support for the assumption that the temporary increase in reduction current was due to the reduction of $Cr^{VI}$. Under the potential and pH conditions of the cell, the probable reducible species are oxygen and $Cr^{VI}$. The reduction of oxygen is not likely to cause a decrease in the overall reduction current over time, whereas the creation of a $Cr^{III}$ film from the reduction of $Cr^{VI}$ should do so. Both Fig. 4 and Table I show that the overall reduction current clearly decreases after the late temporary increase in reduction current. Furthermore, this decrease is more than would be expected by extrapolating the data collected before the temporary increase in reduction current.

**Table I. Current values from chronoamperometry data of Fig. 4, experiment 1.**

| Time elapsed from injection | Reduction current (μA) | Percent decrease in reduction current |
|---|---|---|
| −1 s | −2.415 | ··· |
| 7 m | −0.634 | 73.7 |
| 85 m | −0.217 | 91.0 |
| 4.1 h | −0.136 | 94.4 |
| 7.0 h | −0.121 | 95.0 |
| 9.6 h | −0.158 | 93.5 |
| 14.5 h | −0.073 | 97.0 |
| 23.7 h | −0.010 | 99.6 |

Combining the chronoamperometry experiments and the SERS experiment shown in Fig. 3 suggests a possible cause for the temporary increase and subsequent overall decrease in reduction current. Care should be taken when attempting to extract quantitative data from SERS spectra, as the amount of collected scattering is affected by the proximity of the scattering species to the surface of the substrate and also by the ability of the scattered light to escape from the film, *i.e.*, as a film thickens, the collected scattering can actually decrease. Keeping this caveat in mind, the large increase in the area of the 575 $cm^{-1}$ band coincides chronologically with the increase in current between 5.7 and 16.3 h observed in the chronoamperometry experiments. This dramatic increase in the 575 $cm^{-1}$ band area between 5 and 15 h after the injection was noted in at least three other identically conducted SERS experiments. Furthermore, it is not unreasonable for the SERS effect to show ''long range'' enhancement of molecules tens of nanometers from the surface, a distance which would easily accommodate a bi- or tri-layer.[7] The following sequence of events is consistent with the spectroscopic and electrochemical observations. Within 6 min after injection of $Cr^{VI}$ to

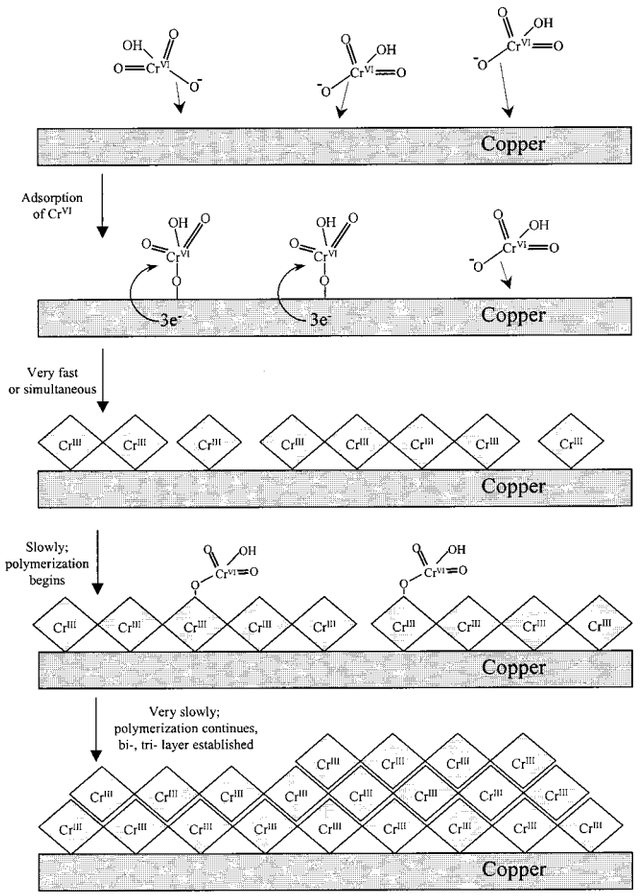


**Figure 5.** Sequence of events during formation of $Cr^{III}$ film.

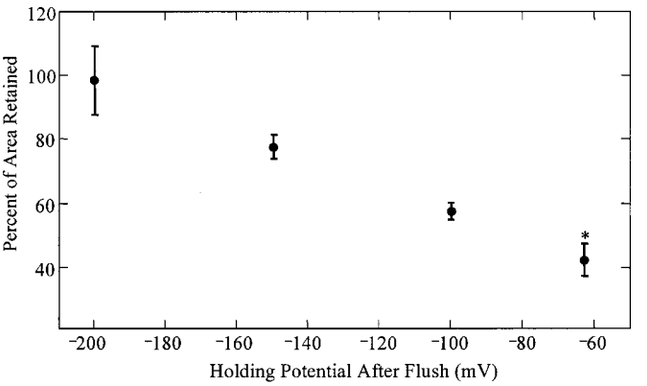


**Figure 6.** Percent of Raman spectral area between 365 and 760 $cm^{-1}$ retained for 5.7 h after $Cr^{VI}$ was removed *vs.* holding potential in flushed cell. *Cell at OCP ($\approx -63$ mV).

the cell, an approximate monolayer of a $Cr^{III}$ film formed and strongly inhibited, but did not completely eliminate, oxygen reduction. As the film continued to form, the reduction of both oxygen and $Cr^{VI}$ contributed to the overall reduction current. Both the reduction of oxygen and the reduction of $Cr^{VI}$ increased the pH at the electrode surface. After approximately 5-10 h, a critical pH value was reached at the surface and the reduction of $Cr^{VI}$ increased for reasons discussed below, and thereby more $Cr^{III}$ formed on the electrode surface. As the film thickened, however, both the further reduction of $Cr^{VI}$ and oxygen reduction were severely inhibited and the overall reduction current dropped to almost zero. Fig. 5 illustrates this sequence of events.

Why would a rise in pH increase the rate of $Cr^{VI}$ reduction? Stunzi *et al.*'s extensive studies of the hydrolytic polymerization of $Cr^{III}$ ions bear on this question.[30-33] As noted in their studies, $Cr^{III}$ almost exclusively and constantly maintains octahedral coordination, with water molecules filling in any of the six positions not otherwise occupied. Although when compared to other metal ion octahedral complexes, $Cr^{III}$ complexes are inert, these studies investigated the relative rates of substitution leading to the formation of $Cr^{III}$ dimers and the further formation of various oligomers. Specifically, Stunzi *et al.* found that deprotonation of complexed water molecules induces a conjugate base effect which leads to significant increases in the rate of replacement and exchange of water molecules at $Cr^{III}$ centers, which in turn increases the rate of oligomer formation.[32,33] Furthermore, King *et al.* discussed the rapid formation of $Cr(CrO_4)(H_2O)_5^+$ and $Cr(HCrO_4)(H_2O)_5^{2+}$ in solutions of $Cr^{III}$ and $Cr^{VI}$ ions.[34] They propose that no breakage of the $Cr^{III}$-O bond occurs, but rather the $Cr^{VI}$-O bond breaks and $Cr^{VI}$ bonds with O-$Cr^{III}$ to make $Cr^{VI}$-O-$Cr^{III}$. The formation of similar bonds with the polymerizing $Cr^{III}$ film could then ultimately lead to the reduction of bonded $Cr^{VI}$. It is, therefore, suggested that the increase in pH brought on by the potential controlled reduction of both oxygen and $Cr^{VI}$ could provide a driving force for the further reduction of $Cr^{VI}$ as a $Cr^{III}$ film polymerizes, explaining the temporary increase in reduction current seen in all three experiments of Fig. 4.

As previously noted, the copper substrate in the above experiments was held at $-200$ mV vs. Ag/AgCl, which is the approximate OCP of AA-2024 T3 in 100 mM $K_2SO_4$. To better understand the stability of the $Cr^{III}$ film, a series of four experiments identical to the SERS experiment, which produced the spectra of Fig. 3, was performed. In each case, the copper substrate was held at $-200$ mV, $Cr^{VI}$ was added to bring the cell $Cr^{VI}$ concentration to $\sim$5.5 mM, and the $Cr^{III}$ film was allowed to grow for 19-24 h at $-200$ mV. Acquired spectra from this initial stage of all four experiments showed essentially the same results as Fig. 3. After 19-24 h, the cell was manually flushed while maintaining the copper electrode at $-200$ mV until a final $Cr^{VI}$ concentration of $\sim$14 $\mu$M $Cr^{VI}$ was reached. At this concentration, the cell is no longer acidic and has a pH of $\sim$7.1. After the cell was flushed, for each of the four experiments, respectively: (*i*) the potential was left at $-200$ mV, (*ii*) the potential was increased to $-150$ mV, (*iii*) the potential was increased to $-100$ mV, or (*iv*) potential control was turned off and the cell was allowed to drift to its OCP, which was previously determined to be approximately $-63$ mV. In each of these four experiments, the flushed cell was maintained under its respective potential for 5.7 h. Spectra were acquired both before and after this holding period. The plot in Fig. 6 was created using four replicate spectra from each of the four experiments. Two of the four spectra were acquired immediately before the cell was flushed and two of the spectra were acquired at the end of the 5.7 h. The spectra were baseline corrected by leveling between 365 and 760 $cm^{-1}$, and the area of the 575 $cm^{-1}$ band was determined by integrating between these same endpoints. Galactic's Grams spectral software (version 4.02) was used to perform baseline adjustments and all integrations. Figure 6 shows the percent of the 575 $cm^{-1}$ band area retained after 5.7 h at each respective holding potential, relative to the 575 $cm^{-1}$ band area before the cell was flushed. The film remained stable at $-200$ mV, however, as the holding potential increased, the area of the 575 $cm^{-1}$ band decreased, indicating less stability for the $Cr^{III}$ film at more positive potentials. Compared to the OCP of AA-2024 T3 under most field conditions, a potential of $-200$ mV is relatively high. For example, the measured OCP of AA-2024 T3 in 100 mM NaCl is $-540$ mV. Therefore, although the $Cr^{III}$ film is only a few

monolayers thick, under near neutral pH conditions and potentials $\leqslant -200$ mV *vs.* Ag/AgCl, it is chemically stable.

A chromium-containing layer of a few monolayers differs greatly in thickness from the several micrometer thick CCC, even though they both originate with $Cr^{VI}$ in solution. Alodine 1200 solution has a much higher $Cr^{VI}$ concentration ($\sim$40 mM) than that studied here, and the $Fe(CN)_6^{3-}$ ''accelerator'' generates a high concentration of $Cr^{III}$ during CCC formation. The $Cr^{III}$ polymerized slowly due to the low pH, so that a sol-gel was formed, containing both $Cr^{III}$ and $Cr^{VI}$. It is likely that many $Cr^{VI}$-O-$Cr^{III}$ bonds were formed in such a sol-gel, and they may have been reduced to $Cr^{III}$-O-$Cr^{III}$ or been incorporated into the CCC as $Cr^{III}/Cr^{VI}$ mixed oxide. The fact that $Cr^{VI}$ is more labile to substitution than $Cr^{III}$ is consistent with an important role of the $Cr^{VI}$-O-$Cr^{III}$ linkage in CCC formation. The lability of $Cr^{VI}$ *vs.* the inertness of $Cr^{III}$ is illustrated by the well-established fast equilibrium: $2HCrO_4^- \rightleftarrows Cr_2O_7^{2-} + H_2O$, and the very low exchange rate constant of $H_2O$ at a $Cr^{III}$ center of $<10^{-5}$ $s^{-1}$.[35] As the sol-gel continued to cross-link, $Fe(CN)_6^{3-}$ and $F^-$ mass transport were presumably decelerated and the CCC thickness became self-limiting. The main factors promoting thick CCC formation are low pH, presence of $Fe(CN)_6^{3-}$, high $Cr^{VI}$ concentration, and the constant exposure of bare aluminum by $F^-$ ion etching. The dilute $Cr^{VI}$ solution studied in the current work had none of these factors present, so electron transfer to either oxygen or $Cr^{VI}$ was inhibited by only a few monolayers. It should be emphasized that both CCC formation and redox inhibition by dilute $Cr^{VI}$ depended on the critical $Cr^{VI}$-O-$Cr^{III}$ intermediate.

## Conclusions

The copper-rich intermetallics that add strength to aluminum alloys make them particularly susceptible to localized corrosion in part by providing cathodic sites for oxygen reduction. The current work provides spectroscopic evidence that a $Cr^{III}$ oxyhydroxide film forms on copper exposed to chromate and that this film severely inhibits oxygen reduction on copper. Although oxygen reduction inhibition is a clear effect of the $Cr^{III}$ film, its general inhibition of electron transfer may also interfere with oxidation reactions associated with anodic dissolution.[36-38] At a potential of $-200$ mV *vs.* Ag/AgCl, a near monolayer of substitution inert $Cr^{III}$ is established on a copper surface within minutes after its exposure to $Cr^{VI}$ solution, and this initial layer decreases oxygen reduction on the copper sites by $>70\%$. Over a period of several hours the further reduction of $Cr^{VI}$ continues to contribute to the $Cr^{III}$ film thickness on the copper surface, with further inhibition of oxygen reduction. The binding of labile $Cr^{VI}$ to the $Cr^{III}$ centers of the film serves to concentrate $Cr^{VI}$ at the alloy surface, and it may provide a conduit for transferring electrons from the alloy to $Cr^{VI}$. As the $Cr^{III}$ film thickens, it effectively shuts down both oxygen reduction and further $Cr^{VI}$ reduction. Under neutral pH conditions and OCP, encountered in field applications, this substitution inert $Cr^{III}$ film is stable. Furthermore, a CCC or $Cr^{VI}$ containing primer provides a ready source of mobile $Cr^{VI}$ which can adsorb and reduce at defects to effect ''self healing.'' Perhaps the most important and distinctive feature of $Cr^{VI}$ is its transition upon reduction from a mobile, substitution labile form to insoluble, substitution inert $Cr^{III}$. The spectroscopic results clearly support a mechanism based on rapid, irreversible $Cr^{VI}$ reduction at cathodic sites, slow subsequent adsorption and reduction of $Cr^{VI}$ to $Cr^{III}$, and eventual formation of a self-limiting layer with a thickness of several $Cr^{III}$ monolayers. The substitution rates of $Cr^{III}$ and $Cr^{VI}$ are critical to the process as is the existence of the $Cr^{VI}$-O-$Cr^{III}$ linkage during Cr deposition. The product of dilute $Cr^{VI}$ interactions with AA-2024 T3 inhibits electron transfer in general, and particularly oxygen reduction on what had been cathodic sites.

## Acknowledgments

This work was supported by the Air Force Office of Scientific Research and the Strategic Environmental Research and Development Program. The authors appreciate informative conversations with Professors Gerald S. Frankel and Rudolph G. Buchheit.

*The Ohio State University assisted in meeting the publication costs of this article.*

## References

1. G. S. Chen, M. Gao, and R. P. Wei, *Corrosion (Houston)*, **52**, 8 (1996).
2. R. G. Buchheit, R. P. Grant, P. F. Hlava, B. Mckenzie, and G. L. Zender, *J. Electrochem. Soc.*, **144**, 2621 (1997).
3. P. L. Hagans and C. M. Haas, *Surf. Interface Anal.*, **21**, 65 (1994).
4. W. R. McGovern, P. Schmutz, R. G. Buchheit, and R. L. McCreery, *J. Electrochem. Soc.*, **147**, 4494 (2000).
5. W. J. Clark, J. D. Ramsey, R. L. McCreery, and G. S. Frankel, *J. Electrochem. Soc.*, **149**, B179 (2002).
6. W. J. Clark and R. L. McCreery, *J. Electrochem. Soc.*, **149**, B379 (2002).
7. Z. Q. Tian, *Internet Journal of Vibrational Spectroscopy*, **4**, 2 (2002).
8. H. Y. H. Chan, C. G. Takoudis, and M. J. Weaver, *J. Phys. Chem. B*, **103**, 357 (1999).
9. L. Xia and R. L. McCreery, *J. Electrochem. Soc.*, **145**, 3083 (1998).
10. K. G. Ray and R. L. McCreery, *Appl. Spectrosc.*, **51**, 108 (1997).
11. K. J. Frost and R. L. McCreery, *Appl. Spectrosc.*, **52**, 1614 (1998).
12. L. Xia, E. Akiyama, G. S. Frankel, and R. L. McCreery, *J. Electrochem. Soc.*, **147**, 2556 (2000).
13. A. Kudelski, M. Janik-Czachor, J. Bukowska, M. Dolata, and A. Szummer, *J. Mol. Struct.*, **482-483**, 245 (1999).
14. H. Yamada, *Appl. Spectrosc. Rev.*, **17**, 227 (1981).
15. J. D. Ramsey and R. L. McCreery, *J. Electrochem. Soc.*, **146**, 4076 (1999).
16. A. G. Schrott, G. S. Frankel, A. J. Davenport, H. S. Isaacs, C. V. Jahnes, and M. A. Russak, *Surf. Sci.*, **250**, 139 (1991).
17. G. P. Halada and C. R. Clayton, *J. Electroanal. Chem. Interfacial Electrochem.*, **138**, 2921 (1991).
18. J. D. Ramsey, L. Xia, M. W. Kendig, and R. L. McCreery, *Corros. Sci.*, **43**, 1557 (2001).
19. J. E. Maslar, W. S. Hurst, W. J. Bowers, Jr., J. H. Hendricks, M. I. Aquino, and I. Levin, *Appl. Surf. Sci.*, **180**, 102 (2001).
20. L. J. Oblonsky and T. M. Devine, *Corros. Sci.*, **37**, 17 (1995).
21. C. A. Melendres, M. Pankuch, Y. S. Li, and R. L. Knight, *Electrochim. Acta*, **37**, 2747 (1992).
22. J. E. Maslar, W. S. Hurst, T. A. Vanderah, and I. Levin, *J. Raman Spectrosc.*, **32**, 201 (2001).
23. H. Y. H. Chan, C. G. Takoudis, and M. J. Weaver, *Electrochem. Solid-State Lett.*, **2**, 189 (1999).
24. N. Cioffi, L. Torsi, I. Losito, C. Di Franco, I. De Bari, L. Chiavarone, G. Scamarcio, V. Tsakova, L. Sabbatini, and P. G. Zambonin, *J. Mater. Chem.*, **11**, 1434 (2001).
25. G. Niaura, *Electrochim. Acta*, **45**, 3507 (2000).
26. F. Texier, L. Servant, J. L. Bruneel, and F. Argoul, *J. Electroanal. Chem.*, **446**, 189 (1998).
27. C. Sunseri, S. Piazza, and F. Di Quarto, *J. Electrochem. Soc.*, **137**, 2411 (1990).
28. S. E. Butler, P. W. Smith, R. Stranger, and I. E. Grey, *Inorg. Chem.*, **25**, 4375 (1986).
29. L. Pejov and V. M. Petrusevski, *Spectrochim. Acta, Part A*, **56**, 947 (2000).
30. H. Stunzi and W. Marty, *Inorg. Chem.*, **22**, 2145 (1983).
31. H. Stunzi, F. P. Rotzinger, and W. Marty, *Inorg. Chem.*, **23**, 2160 (1984).
32. F. P. Rotzinger, H. Stunzi, and W. Marty, *Inorg. Chem.*, **25**, 489 (1986).
33. H. Stunzi, L. Spiccia, F. P. Rotzinger, and W. Marty, *Inorg. Chem.*, **28**, 66 (1989).
34. E. L. King and J. A. Neptune, *J. Am. Chem. Soc.*, **77**, 3186 (1955).
35. B. Douglas, D. McDaniel, and J. Alexander, *Concepts and Models of Inorganic Chemistry*, John Wiley & Sons, Inc, New York (1994).
36. G. O. Ilevbare, J. R. Scully, J. Yuan, and R. G. Kelly, *Corrosion (Houston)*, **56**, 227 (2000).
37. G. O. Ilevbare and J. R. Scully, *J. Electrochem. Soc.*, **148**, 196 (2001).
38. G. O. Ilevbare and J. R. Scully, *Corrosion (Houston)*, **57**, 134 (2001).